Notch-Tip Strain Fields in an Aluminum Sheet with Serrated Plasticity

W. Tong, Y. Xuan
Southern Methodist University, Dallas, Texas, U.S.A.

1. Introduction

Al-Mg aluminum alloys such as AA5052-H32, AA5083-H116 and AA5182-H19 often show serrated plastic flow behavior due to the so-called dynamic strain ageing (DSA) or Portevin-Le Chatelier (PLC) effect [1,2]. Such an effect on the notch-tip strain fields and subsequent crack initiation and propagation receives only limited attentions [3-7]. Early works focus on the possible role of DSA on the tearing failure characteristics in aluminum sheets or plates [1,2] and more recent works emphasize both experimental strain field measurements and numerical simulation of aluminum samples with straight and/or tapered as well as U- and/or V-notched gage sections [3-7].

There are clearly some differences in the deformation behaviors between the conventional tension coupons and notched coupons from the experimental investigations and numerical simulations. While load serrations were clearly observed in the testing of dog bone-shaped tension coupons made of flat sheets, no or very small load serrations were detected in the testing of V-notched coupons of flat sheets [3,5,7]. However, the crack propagation was found to advance in an intermittent manner in the V-notched coupon under slow but constant crosshead speeds using a hard test machine [3]. On the other hand, load serrations were found to increase significantly with the decreasing notch radius in the U-notched cylindrical bars [6]. No load serrations was detected experimentally for the sharp U-notched flat sheet made of a Al-4%wt Cu binary alloy although localized plastic strain rate bands were predicted by the numerical simulations [4]. Furthermore, very complex patterns of localized plastic strain rate bands have also been predicted for V-notched coupons by the numerical simulations [5].

In the present work, the effect of test coupon geometries (straight gage section of tension coupons and U- and V-notched coupons of thin sheets) on the characteristics of overall load serrations and local strain rate fields are further studied experimentally using a *soft* testing machine. The use of the soft (compliant) testing machine instead of a hard (stiff) testing machine is intended to enhance the sensitivity in detecting any possible load serrations during each test. The local strain rate fields are measured by the time-resolved digital imaging and associated image correlation analysis [8,9]. In the following, the experimental details will be described first. The results of load serrations and selected local strain rate fields in the tension testing of the conventional straight-gage section coupons using both hard and soft testing machines will be presented. Similar results on the U- and V-notched test coupons on the soft testing machine will then

be given and compared against those of the tension test coupons. Conclusions of the current experimental investigation will be presented at the end.

2. Experimental Details

The material in this study is a thin gage AA5182-H19 sheet supplied by Alcoa, Inc. (Pittsburgh, PA). The sheet thickness is 0.28mm and the test coupons were machined in such a way the axial tension loading direction is parallel to the rolling direction of the sheet. Three types of the test coupons were used in the current experimental investigation. Type 1 coupon is of the conventional dog-bone shaped uniaxial tension coupon with a straight gage section (total length: 50mm long; gage section: 22mm long and 5mm wide; the width of its two gripping ends: 10mm wide). Type 2 coupon is double edge U-notched (total length: 50mm long; gage section between the grippers: 32 mm long and 7.5mm wide; semicircular notches of 5mm in diameter). Type 3 coupon is double edge 90-deg V-notched (total length: 50mm long; gage section between the grippers: 32 mm long and 7.5mm wide).

Uniaxial tension tests were carried out on two different Instron material testing machines models 5582 and E1000, respectively (Canton, MA). A constant crosshead speed of 0.01 mm/s was used in the tests done on both the Instron machine 5582 with machine-specimen stiffness of 2800 N/mm and the E1000 machine with auto-tuned machine-specimen stiffness of 1700 N/mm. Both machines recorded the time, axial extension (displacement) and axial load data at a rate of 50 Hz. Both U-notched and V-notched test coupons were tested to fracture only on the Instron E1000 machine under the conditions similar to the uniaxial tension tests.

In addition, a compact high-speed digital camera by Visions Research Inc. (Phantom camera model Miro 4) was used to image one of the flat surfaces of the test coupons during the testing. The surface of each test coupon was decorated with finely sprayed black paint speckles and the 8-bit grayscale digital images were recorded at a frame rate of 30 frame/s in this study. The digital images were subsequently analyzed using a digital image correlation program for extracting the whole-field strain field data [8,9]. In particular, when the adjacent pairs of image frames were analyzed, the obtained strain increment can be regarded as the result of the average strain rate between the two image frames multiply the time interval of 1/30 second.

3. Results and Discussions

3.1 Plastic Deformation Behavior

First, the experimental results of the uniaxial tension tests on AA5182-H19 sheet metal are presented in Fig.1 and Fig.2 using Instron testing machines 5582 and E1000 respectively. As shown in Fig.1(a), the load-time curve (red line) exhibits many high frequency serrations shortly after the test time of 60 seconds. Those

serrations are commonly seen in tension tests using hard (stiff) testing machine under displacement control [3-7,9]. A constant crosshead speed of 0.01mm/s was achieved according to the displacement-time curve (the blue line) shown in Fig.1(a). Each serration (load drop) corresponds to the nucleation and growth a narrow plastic deformation band (the so-called PLC band of type B or C). Fig.1(b) show the four plastic strain increment maps (on the left side) that correspond to the first four load serrations in the tension coupon. It indicates that the PLC bands initiated first at the root of the shoulder section of the tension coupon and the orientation of the bands are more or less perpendicular to the (horizontal) axial loading direction. Once the location of the deformation bands moves towards the center portion of the gage section, the deformation band is found to inclined with a certain angle of about 55 deg with respect to the tensile axis [3,9].

However, the experimental results obtained from the uniaxial tension tests of AA5182-H19 using a soft testing machine (Instron E1000 machine) are quite different, see Fig.2 (a). Large load drops with lower frequency (instead of high-frequency low amplitude load serrations shown in Fig.1a) were seen in the load-time curve (the blue line in Fig2a). Interestingly, the recorded displacement-time curve (the red line in Fig.2a) show large spikes at the times of the large load drops. Some selected strain increment maps corresponding to the load drops and displacement spikes are shown in Fig.2(b). In general, the deformation zone is much large than the individual deformation bands shown in Fig.1(b) and the strain level per increment is about one order higher.

The large spikes in displacement-time data are results of the characteristics of the Instron E1000 testing machine under displacement control with stiffness-based loop tuning mechanism (for trying to maintain a constant loading train stiffness response dynamically). In other words, the small load serrations in AA5182-H19 tension coupon (see Fig.1a) would induce the overly compensated displacement control towards a constant loading rate (instead of a constant crosshead speed) and subsequently large load drops. It concludes that E1000 testing machine may be used advantageously to enhance the sensitivity in detecting small load serrations in a test involved U- or V-notched coupons.

3.2 Results of U- and V-Notched Coupons

Representative results of tension testing of U- and V-notched AA5182-H19 test coupons are shown in Fig.3 and Fig.4, respectively. Both load drops as well as displacement spikes were detected for the U-notched coupons (see Fig.3a) and the local strain increment were found to be relatively high and extend almost over the entire width of the notched region (Fig.3b). On the other hand, only small load drops were seen for the V-notched coupons and small or no displacement spikes were detected (Fig.4a). The corresponding local strain increment maps for the V-notched coupons show only a more localized strain field around one of the notch tip and it does not usually extend across the entire width of the notched region (see Fig.4b).

4. Conclusions

By using the Instron's newly developed Electropuls E1000 machine for uniaxial tension testing under displacement control, much larger load drops as well as large displacement spikes were detected for AA5182-H19 sheet coupons with serrated plastic flow behavior. Consequently, such a testing methodology was used to test both U-notched and V-notched test coupons made of the same sheet metal materials. Clearly observable load drops were detected in both types of the notched coupons but the magnitude is much smaller for the V-notched coupons than those of U-notched coupons. The strain increment maps measured from the digital image correlation method indicate that the strain field around the notch tips spreads out much more across the width of the test coupon when there is a clearly detectable load drop. When a plastic deformation field develops only in a highly localized manner (say around a sharp V-notched tip), small or no load serrations would be appear in the overall load-displacement record.

References

[1] J.E. King, C.P. You, J.F. Knott, Serrated yielding and the localized shear failure mode in aluminum alloys, Acta Metallurgica 29(9) (1981) 1553-1566

[2] D. Delafosse, G. Lapasset, Kubin, L.P. Kubin, Dynamic strain ageing and crack propagation in the 2091 Al-Li alloy, Scripta Metallurgica et Materialia 29(11) (1993) 1379-1384

[3] W. Tong, N. Zhang, On the crack initiation and growth in a strongly dynamic strain aging aluminum alloy sheet, Journal of Materials Science and Technology, 20(Suppl.) (2004) 23-26

[4] S. Graff, S. Forest, J.-L. Strudel, C. Prioul, P. Pilvin, J.-L. Bechade, Strain localization phenomena associated with static and dynamic strain ageing in notched specimens: Experiments and finite element simulations, Materials Science and Engineering A387-389(1-2) (2004) 181-185

[5] S. Graff, S. Forest, J.-L. Strudel, C. Prioul, P. Pilvin, J.-L. Bechade, Finite element simulations of dynamic strain ageing effects at V-notches and crack tips, Scripta Materialia 52 (2005) 1181-1186

[6] A. Benallal, T. Berstad, T. Borvik, A.H. Clausen, O.S. Hopperstad, Dynamic strain aging and related instabilities: experimental, theoretical and numerical aspects, European Journal of Mechanics A/Solids 25(3) (2006) 397-424

[7] A. Benallal, T. Berstad, T. Borvik, A.H. Clausen, O.S. Hopperstad, I. Koutiri, R. Nogueira de Codes, An experimental and numerical investigation of the behavior of AA5083 aluminum alloy in presence of the Portevin-Le Chatelier effect, Int. J. Plasticity 24 (2008) 1916-1945

[8] W. Tong, An evaluation of digital image correlation criteria for strain mapping applications, Strain 41(4) (2005) 167-175

[9] W. Tong, N. Zhang, On the serrated plastic flow in an AA5052-H32 sheet, ASME J. Eng. Mater. Tech. 129(2) (2007) 332-341

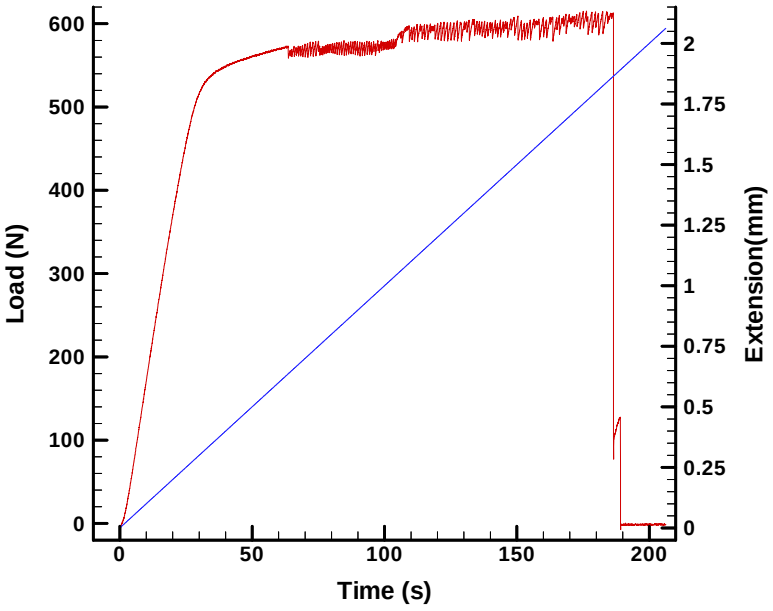

(a)

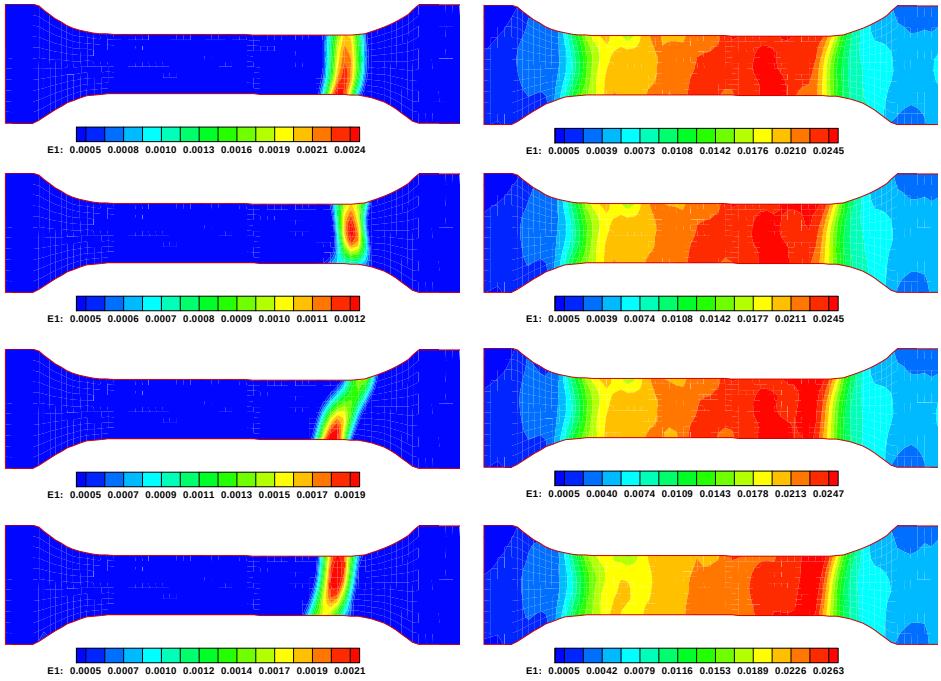

(b)

Figure 1 Experimental results of a tension test on AA5182-H19 flat coupon using a hard (stiff) testing machine Instron Model 5582: (a) force-displacement-time curves; (b) selected local axial strain increment maps (left) and the cumulative total axial strain maps (right) of the first four load serrations.

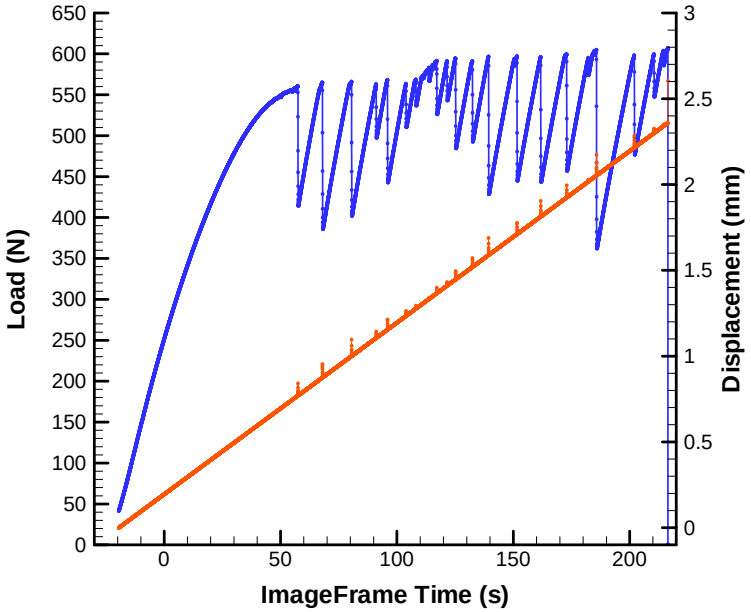

(a)

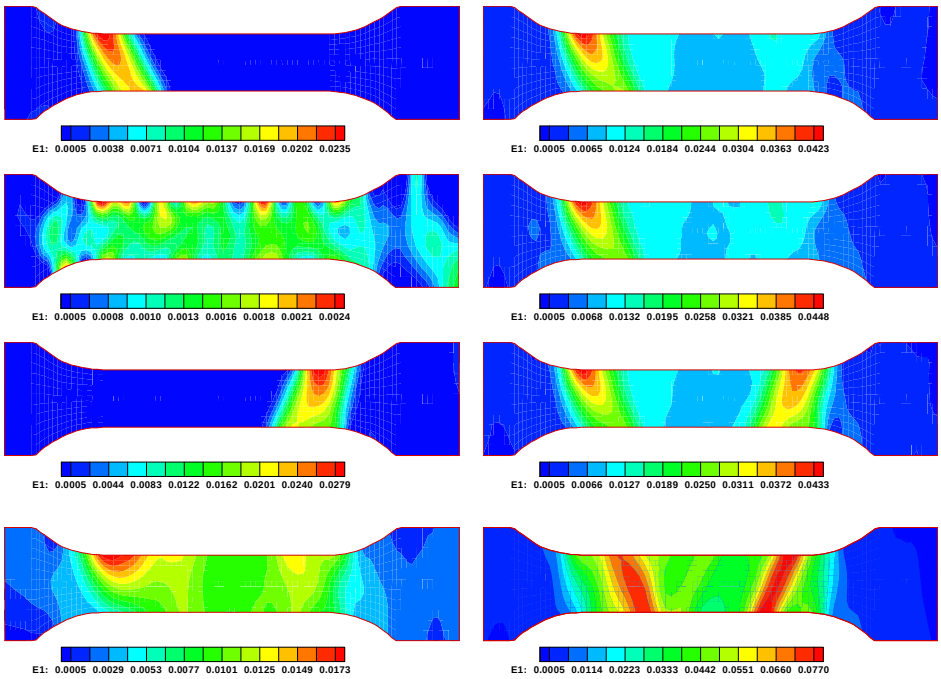

(b)

Figure 2 Experimental results of a tension test on AA5182-H19 flat coupon using a soft (compliant) testing machine Instron Model E1000: (a) force-displacement-time curves; (b) selected local axial strain increment maps (left) and the cumulative total axial strain maps (right) of the first four major load serrations.

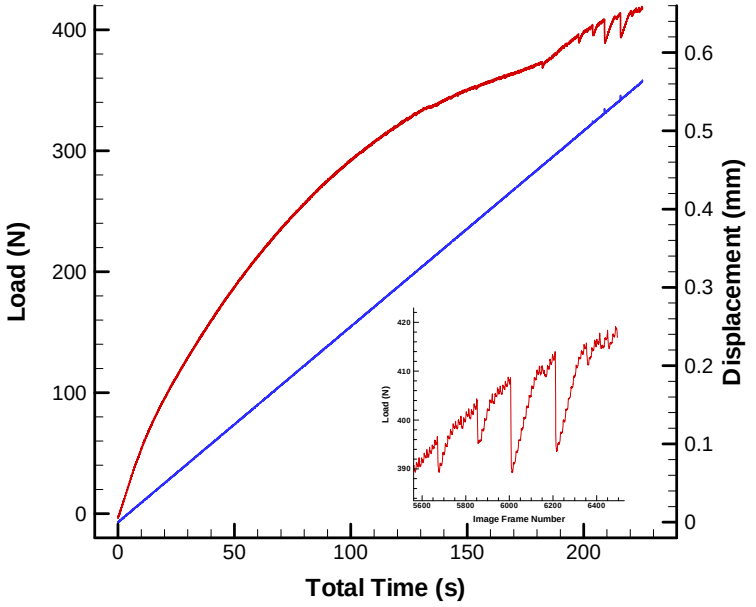

(a)

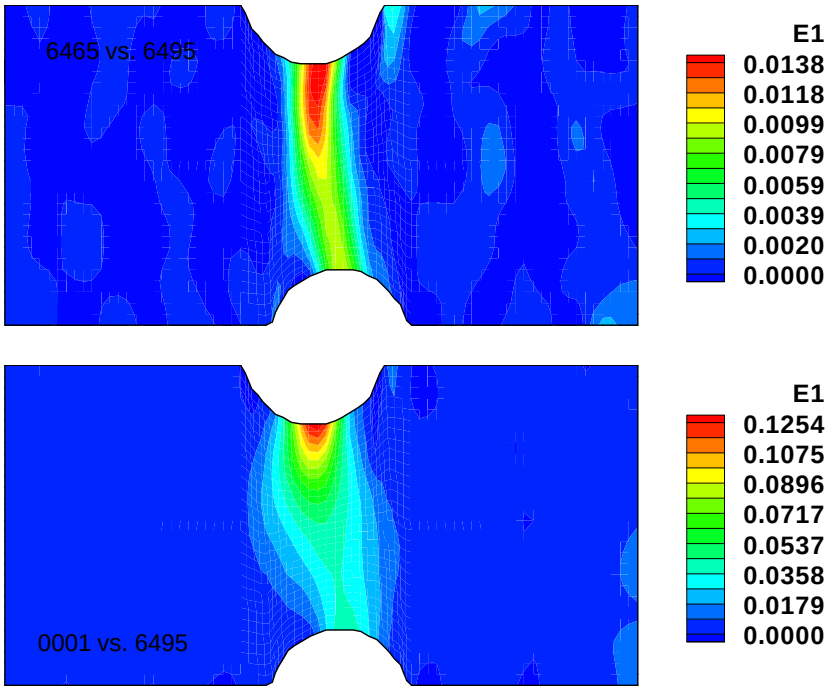

(b)

Figure 3 Experimental results on a double edge U-notched AA5182-H19 flat coupon using a soft (compliant) testing machine Instron Model E1000: (a) force-displacement-time curves; (b) a selected local axial strain increment map (upper) and the cumulative total axial strain map (lower) of the last major load serration.

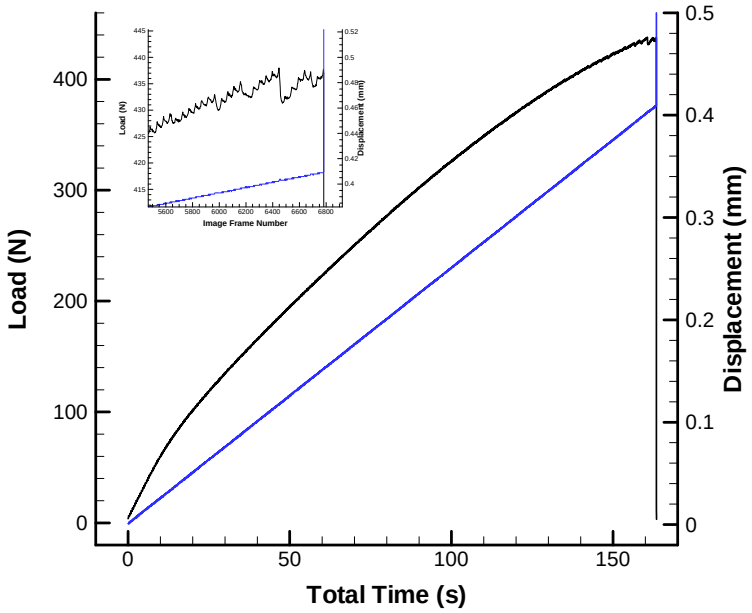

(a)

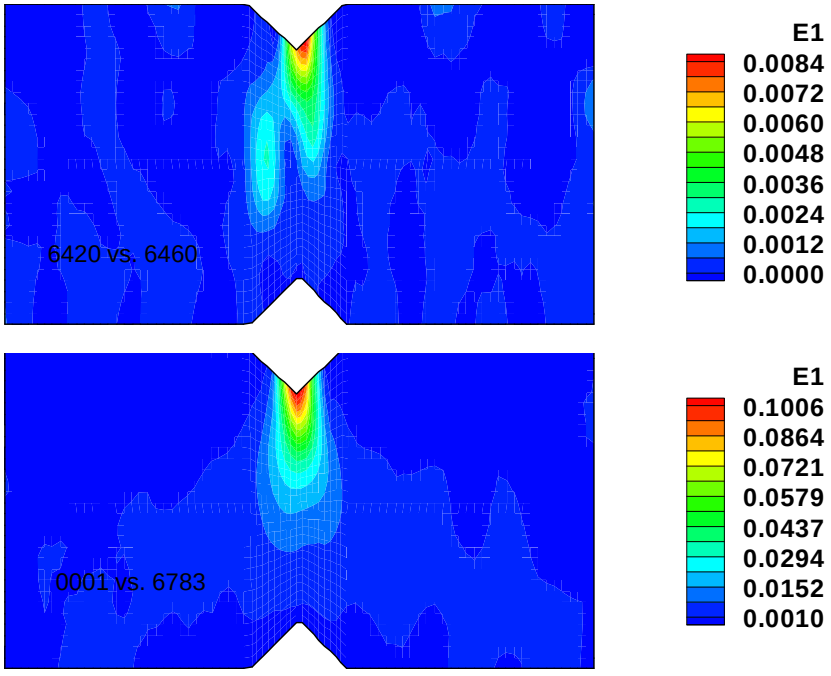

(b)

Figure 4 Experimental results on a double edge V-notched AA5182-H19 flat coupon using a soft (compliant) testing machine Instron Model E1000: (a) force-displacement-time curves; (b) a selected local axial strain increment map (upper) and the cumulative total axial strain map (lower) of the last major load serration.